frontiers | Frontiers in Materials

TYPE Original Research
PUBLISHED 10 April 2024
DOI 10.3389/fmats.2024.1379941

OPEN ACCESS

EDITED BY
Babatunde Okesola,
University of Nottingham, United Kingdom

REVIEWED BY
Idalina Vieira Aoki,
University of São Paulo, Brazil
Evangelia Vouvoudi,
Aristotle University of Thessaloniki, Greece

*CORRESPONDENCE
Zhihui Liu,
liu_zh@jlu.edu.cn

RECEIVED 31 January 2024
ACCEPTED 25 March 2024
PUBLISHED 10 April 2024

CITATION
Li S, Qi L and Liu Z (2024), Antimicrobial properties and bonding durability of pH-responsive dentin adhesives with chlorhexidine-load mesoporous silica nanoparticles.
Front. Mater. 11:1379941.
doi: 10.3389/fmats.2024.1379941

Antimicrobial properties and bonding durability of pH-responsive dentin adhesives with chlorhexidine-load mesoporous silica nanoparticles

Sining Li[1,2], Le Qi[1,2] and Zhihui Liu[1,2]*

[1]Hospital of Stomatology, Jilin University, Changchun, China, [2]Jilin Provincial Key Laboratory of Tooth Development and Bone Remodeling, Changchun, China

In this study, we synthesized pH-sensitive CHX@SBA-PDA nanoparticles and characterized their structure. These nanoparticles were then incorporated into Single Bond 2 commercial dentin adhesive. Subsequently, timely and long-term antibacterial evaluation, cytotoxicity evaluation and bonding properties were conducted. The results demonstrated the successful synthesis of CHX@SBA-PDA nanoparticles. Moreover, CHX@SBA-PDA exhibited excellent pH sensitivity and maintained a high release rate of chlorhexidine (CHX) under cariogenic low pH conditions. At pH 5.0, the release rate could reach up to 71.1% after 24 h of incubation with CHX@SBA-PDA nanoparticles. Among the different adhesive formulations tested, the 2% wt adhesive displayed the strongest immediate and 30 days bacterial inhibition ability ($p < 0.05$). No significant difference was observed in immediate shear strength among the four groups ($p > 0.05$). After undergoing pH cycling, all functional adhesive groups exhibited higher shear strength compared to the control group ($p < 0.05$). Furthermore, there was no significant difference in cell proliferation activity between the experimental group and control group ($p > 0.05$). In conclusion, our functional dentin adhesive containing CHX@SBA-PDA nanoparticles demonstrated long-term antibacterial properties as well as improved bond strength characteristics, thus, offering a promising approach to enhance durability of bonded restorations.

KEYWORDS

dentin bonding, mesoporous silica nanoparticles, chlorhexidine, pH-sensitive, drug delivery

1 Introduction

Dental caries is a bacterial infectious disease and one of the most prevalent human diseases (Pitts et al., 2017). The World Health Organization has identified it as one of the three primary diseases requiring prevention and treatment, along with tumors and cardiovascular diseases (Williams, 2014). The standard treatment for dental caries involves extracting decayed tooth tissue and filling the resulting cavity with restorative materials. Resin composites have emerged as the predominant choice for dental restoration due to its superior aesthetics, biocompatibility and mechanical properties (Simecek et al., 2009; Stewart et al., 2018). However, resin composites are associated with a certain failure rate primarily attributed to secondary caries at the resin-dentin interface (Takahashi and Nyvad,

2011; Ferracane, 2017; Eltahlah et al., 2018). The research findings indicate that the failure rate of resin composites is 15%–50% (Opdam et al., 2010). Not only does the restoration of failed restorations result in increased dental costs, but replacement and repeated restoration can also lead to further loss of tooth structure, trapping patients in a cycle known as the "death spiral" and potentially resulting in eventual tooth loss (Spencer et al., 2010; Liu et al., 2011; Garcia et al., 2020). It is imperative to extend the lifespan of dental restorations and reduce secondary caries through effective inhibition of carcinogenicity, particularly among populations at high risk for cavities. Therefore, there is a critical need for antibacterial dental materials that can effectively combat bacteria responsible for causing secondary caries.

Chlorhexidine (CHX) is a widely used cationic antibacterial agent against oral microorganisms and serves as the gold standard for combating dental biofilms (Poppolo Deus and Ouanounou, 2022). CHX exhibits excellent inhibitory effects on various Gram-positive and Gram-negative bacteria as well as fungi, owing to its ability to interact with negatively charged phospholipids and lipopolysaccharides present in the bacterial cell wall or outer membrane. Moreover, it demonstrates good biological safety (Abdelmonem et al., 2019). To achieve antibacterial purposes, CHX has been incorporated into diverse dental materials (Prado et al., 2023; Alansari et al., 2024). However, direct addition of CHX to dental materials can result in an explosive release of CHX, leading to a rapid decline in their antibacterial properties and formation of pores that adversely affect their mechanical properties (Anusavice et al., 2006; Geraldeli et al., 2021). It is crucial to note that prolonged administration of CHX may induce resistance and reduce microbial diversity specifically in *Streptococcus mutans* (Solderer et al., 2019; Huang et al., 2022), hence continuous administration is not recommended. Consequently, adding CHX directly to dental materials is considered undesirable.

Mesoporous silica nanoparticles, with their stable structure, appropriate pore size, large specific surface area, and outstanding biocompatibility, have been demonstrated to be the superior nanoparticle delivery system for sustained drug release (Budiman et al., 2024). Specifically, Santa Barbara Amorphous-15 (SBA-15), as a commonly used mesoporous silica material, exhibits a remarkably regular hexagonal pore structure with an exceptional loading capacity and pore volume (Takamori et al., 2019). Recent investigations have indicated that Mesoporous silica nanoparticles exhibit tremendous potential as drug carriers in various dental materials. In glass ionomer cement or other restorative materials, mesoporous silica nanoparticles can effectively transport a substantial amount of CHX to enhance its antibacterial activities without compromising the mechanical properties of the materials (Zhang et al., 2014; Yan et al., 2017). Moreover, apart from serving as mere drug carriers, mesoporous silica nanoparticles can be personalized and modified to react to diverse stimulus and perform controlled drug release based on alterations in the microenvironment (Li et al., 2023; Xu et al., 2023). Given that cariogenic bacteria can create an acidic environment, pH-responsive systems hold great significance in preventing secondary caries following restorative treatment. These carriers enable precise antimicrobial release in a pH-dependent manner. The biomimetic polymer of mussel adhesion protein, known as polydopamine, exhibits remarkable adhesive properties, excellent biocompatibility, and robust degradation in weak acid environments (Wu et al., 2021; Wu et al., 2023). Hence, we utilized the oxidative self-polymerization of dopamine to create a pH-responsive polydopamine shell membrane on the surface of SBA-15 for drug release control. At neutral pH, drug molecules are confined within SBA-15 but are released at lower pH levels. Consequently, the integration of CHX@SBA-PDA selectively releases drugs upon acid stimulation, effectively eradicating bacteria.

The objective of this experiment was to synthesize pH-sensitive CHX@SBA-PDA nanoparticles, with polydopamine serving as a "gatekeeper" for precise drug release control, thereby enhancing the antibacterial efficacy of CHX. Additionally, the incorporation of CHX@SBA-PDA nanoparticles into dental adhesives aimed to investigate their pH-responsive release behavior, antibacterial properties, and impact on bond strength. These findings provide valuable insights and experimental evidence for the development and application of functional adhesives.

2 Materials and methods

2.1 Fabrication of nanoparticles and functional adhesive

The dried 1 g SBA-15 (XFNANO, China) was weighed and dispersed into 15 mL of absolute ethanol containing 0.3 M CHX (Sigma, United States). The mixture was ultrasonicated for 10 min, stirred on a magnetic stirrer at 25 °C, 600 rpm for 72 h, and then centrifuged with a high-speed centrifuge (CR21N, Hitachi, Japan) at 25 °C, 10,000 rpm for 10 min to collect the CHX@SBA product. The product was washed three times with absolute ethanol, and the supernatant was collected and vacuum-dried to obtain a white powder of CHX@SBA. 50 mg of CHX@SBA and 100 mg of hydrochloride dopamine were dispersed into 50 mL of Tris-HCl buffer (pH 8.5, 10 mM). The mixture was stirred in a dark environment for 24 h. Subsequently, the mixture was centrifuged with a high-speed centrifuge (CR21N, Hitachi, Japan) at 25 °C, 10,000 rpm for 10 min, washed several times with deionized water to remove excess dopamine, and finally lyophilized.

The experiment was divided into four groups, and CHX@SBA-PDA was added into the commercial adhesive Single Bond 2 (3M ESPE, United States) at mass fractions (wt%) of 0%, 0.5%, 1%, and 2% respectively, and then mixed at 2000 rpm for 60 s. Subsequently, it was stored under light-free conditions at a temperature of 4 °C.

2.2 Characterization of the nanoparticles

The surface morphology of MSN, CHX@SBA-PDA nanoparticles studied by field emission scanning electron microscopy (SEM; SU8020, Hitachi, Japan). Fourier transform infrared spectroscopy (FTIR; Nicolet6700, Thermo, United States) was used to detect the composition and structure of the nanoparticles with a scanning resolution of 4 cm^{-1}, a total of 32 scans, and a range from 400 to 4,000 cm^{-1}. The adsorption and desorption capacity of nitrogen were determined using a fully automated pore size analyzer (Autosorb-IQ, America). The degassing temperature was 200 °C and the degassing time was 8 h.

The specific surface area of nanoparticles was calculated using the BET method, and the nanoparticle pore size and pore volume were determined using the BJH method.

2.3 Drug loading and release

During the preparation of CHX@SBA, the entire supernatant was collected and the concentration of CHX loaded in CHX@SBA was determined using a UV-visible spectrophotometer (Lambda 25, PerkinElmed, United States) at 289 nm, following a pre-corrected fitting line. In addition, the drug loading capacity and drug entrapment efficiency were analyzed using the following equations respectively:

$$\textit{Loading content}\,(\%) = m_0 - m_1/m_2 \times 100$$

$$\textit{Encapsulation efficiency}\,(\%) = m_0 - m_1/m_0 \times 100$$

Where, m_0, m_1, and m_2 respectively represent the mass (in g) of CHX used for synthesizing nanoparticles, the mass (in g) of CHX in the supernatant, and the mass (in g) of CHX@SBA.

The CHX@SBA-PDA (10 mg) was immersed in 5 mL of artificial saliva at pH 7.4 and pH 5.0, respectively, and subjected to agitation in a thermostatic shaker at 37 °C with a shaking frequency of 100 Hz. Subsequently, at intervals of 1, 3, 5, 10, 15, 20, and 25 h, 2 mL of the extract were removed and replaced with an equivalent volume of entirely novel artificial saliva. After centrifugation, the supernatant was measured with a UV-visible spectrophotometer (Lambda 25, PerkinElmed, United States) at 289 nm to evaluate the release profile of CHX over time. This experimental procedure was repeated three times.

2.4 Antibacterial tests *in vitro*

2.4.1 Preparation of the bacterial suspension

The frozen strain *Streptococcus mutans* (UA159) was revived and single colonies were selected in brian heart infusion medium (Solarbio, China) following identification. Subsequently, they were incubated at 37 °C in a 5% CO_2 environment for 24 h. For preservation, the concentration of the bacterial solution was adjusted to 1×10^6 CFU/mL.

2.4.2 Adhesion plate bacterial colony counting

The samples (round, r = 1 cm, n = 6) were immersed in artificial saliva for 24 h and 30 days, respectively. After drying and sterilization, they were co-cultivated with a 2 mL bacterial solution for 48 h. Subsequently, the samples were removed and rinsed three times with sterile PBS to eliminate unadhered bacteria. Then, 2 mL of fresh medium was added and subjected to ultrasonic shock for 10 min to ensure complete introduction of all bacteria into the medium. The bacterial solution was diluted to a specific ratio using a step-by-step dilution method. An appropriate amount of the diluted bacterial solution was taken and uniformly coated onto sterile brain heart infusion agar plates using coating sticks. The plates were then incubated for 48 h followed by colony counting.

2.4.3 Live/dead bacterial staining

The sample was co-cultured with the bacterial solution for 48 h. The live/dead bacteria kit (Thermo Science Fisher, United States) was used for staining, and the staining solution was made by mixing SYTO 9 and PI in a 1:1 ratio. Subsequently, each well received 1 mL of the staining solution, which was added while the light was shielded, and it was incubated for 20 min. Afterward, the staining solution was then extracted, followed by two gentle washes with sterile PBS. Finally, observation and photography were conducted using a fluorescence microscope (Olympus, Japan).

2.4.4 SEM of the bacteria attached to the sample surface

The sample, which has been immersed in deionized water for a duration of 30 days, was retrieved and subjected to co-cultivation with the bacterial solution for a period of 48 h. Subsequently, the co-cultured sample was fixed using 2.5% glutaraldehyde (Solarbio, China) at a temperature of 4 °C for a duration of 4 h. Dehydration of the sample was accomplished through dehydrated with a gradient ethanol series (30%, 50%, 70%, 80%, 90%, 95%, and finally 100%), with each concentration being repeated twice for a time span of 15 min per repetition. Finally, the specimen was lastly dried and sprayed with gold before observation.

2.5 Shear bond strength test

Selected orthodontically extracted adult premolars or molars (n = 12) were approved by the Human and Animal Research Ethics Committee (JDKQ 2024). The enamel of the crown was excised with a low speed diamond cutting machine (SYJ-150, China) to expose the dentin, which was polished under running water with 180 mesh, 360 mesh, and 600 mesh sandpaper, respectively, to simulate the hybrid layer. 37% phosphoric acid (Heraeus Kulzer GmbH, Germany) was used to etch the dentin for 30 s. The Single Bond 2 adhesive (3M ESPE, United States) was utilized and cured in accordance with the provided instructions, and then, the cylindrical plastic mold (r = 2 mm) was securely affixed onto the dentin surface treated with the adhesive. Z350XT resin composites (3M ESPE, United States) was then placed into the molds using the gradual placement technique, and each layer was allowed to cure for 40 s. The bonded specimens were split into two groups, the first group were immersed in pH 7.4 artificial saliva for a duration of 24 h, while those in the second group was challenged with pH challenge (immersed in artificial saliva at pH 7.4 for 23 h and in artificial saliva at pH 5.0 for 1 h for 30 days). Subsequently, the specimens were subjected to shear bond strength testing utilizing a universal testing apparatus (AG-X plus, Shimadzu, Japan). This machine applied a constant cross-head speed of 1 mm/min until failure of the sample occurred. The chisel-shaped end of the instrument was designed with a flat contact surface parallel to the dividing line between dentin and the resin composites. The calculation of the shear bonding strength in megapascals (MPa) was performed by dividing the peak load at the point of failure by the area of bonding.

After completion of the shear strength test, both the fracture site on the tooth surface and the resin post were examined under a stereomicroscope (Olympus SZX16, Japan) to observe the fracture pattern. Based on the location of the fracture surface, bond failure

patterns were classified into three types: adhesive fractures, cohesive fractures and mixed fractures.

2.6 Cell compatibility test

2.6.1 CCK8 assay

The cytotoxicity test was conducted using the CCK 8 assay. Human gingival fibroblasts (HGFs) were used for the experiment, and the cells were cultured in Dulbecco's modified Eagle's medium (DMEM) (HyClone, United States) supplemented with 10% (v/v) heat inactivated fetal bovine serum (Bioind, Israel) and 1% (v/v) penicillin-streptomycin (HyClone, United States) in a humidified 5% CO_2 atmosphere at 37 °C. The prepared samples were placed in 6-well plates, and DMEM was added at a ratio of 3 cm^2/mL to the surface area of the specimen, and after 24 h, the extract was collected. Subsequently, serial dilutions of the extract were made with medium at ratios of 1:1,000, 1:2000, and 1:4,000 (v/v). Cells were then planted at a density of 5×10^3 cells per well in 96-well plates and cultured for another 24 h. Following this incubation period, the extract was replaced and further incubated for an additional 24 h. As per the instructions provided by CCK 8 protocol guidelines, CCK 8 reagent (Beyotime, China) was applied to each well and allowed to incubate for a period of 2 h. Finally, absorbance measurements were taken using a plate reader (BL340, Biotech, United States) set at a wavelength of 490 nm.

2.6.2 Live/dead cell staining

The cell activity was assessed using the extract. Logarithmically grown HGFs were cultivated in 6-well plates at a density of 5×10^4 cells per well and cultivated for 24 h. Subsequently, the cells were exposed to the extract and left to incubate for a further 24 h. The cells were stained in accordance with the directions of the calcein/PI cell viability/cytotoxicity assay kit (Beyotime, China), which were then observed under fluorescence microscopy.

2.7 Statistical analysis

The statistical analysis of all data was conducted using SPSS software (version 27.0, SPSS Inc., United States). The colony count, shear strength, and CCK 8 assay results were reported as mean ± standard deviation. One-way ANOVA and Tukey's test were employed to analyze the experimental outcomes. Statistical significance was defined as $p < 0.05$.

3 Results

3.1 Characterization of the nanoparticles

The preparation and utilization of CHX@SBA-PDA nanoparticles are illustrated in Scheme 1. Representative SEM images, EDS elemental mapping and Element mapping of the nanoparticles are shown in Figure 1. SEM revealed that SBA-15 exhibited a well-defined hexagonal pore structure, with clustered and arranged particles, showcasing the characteristic morphology of SBA-15. The surface of SBA-15 appeared smooth with clear edges, while irregular small particles were observed on the surface of CHX@SBA-PDA, indicating adsorption of the drug on both the outer surface and within the mesopores of SBA-15. Additionally, a polydopamine coating was formed on SBA-15. Notably, CHX@SBA-PDA displayed an uneven surface with indistinct edges and significantly larger diameter compared to pristine SBA-15. Energy-dispersive X-ray spectroscopy (EDS) results demonstrated uniform distribution of carbon (C), nitrogen (N), oxygen (O), silicon (Si), and chlorine (Cl) elements within the complex CHX@SBA-PDA.

FT-IR spectroscopy was employed to confirm the composition and structure of the nanoparticles. As shown in Figure 2, the characteristic peaks of SBA-15 were observed at 1,089 cm^{-1} and 802 cm^{-1}, corresponding to the asymmetric stretching vibration, symmetric stretching vibration, and bending vibration of Si-O-Si bond. The stretching vibration peak of Si-OH was detected at 3,460 cm^{-1}. The absorption peak remained essentially unchanged before and after drug loading, indicating the preservation of the mesoporous silicon material's skeletal structure throughout the process. Characteristic peaks associated with CHX were identified at 2,940 cm^{-1}, 1850 cm^{-1}, and 1,090 cm^{-1}, representing C-H and C-N stretching vibrations. Physical loading of CHX into SBA-15 resulted in a nearly masked characteristic band for CHX. In this study, a peak similar to that of CHX appeared for CHX@SBA while the original band largely disappeared, this appearance can be attributed to residue on the surface as confirmed by SEM results. Following polydopamine modification, a contraction vibration resulting from C=C (1,675–1,640 cm^{-1}) within indole-based structures emerged at 1,640 cm^{-1} along with a broad stretch band caused by NH/OH tensile vibrations ranging from 3,100 to 3600 cm^{-1}, these observations indicate successful formation of polydopamine coating.

The porous structure was characterized using nitrogen adsorption and desorption techniques. As shown in Figure 3, the isotherm of SBA-15 was of Type IV, accompanied by a Type H1 hysteresis loop due to capillary condensation of nitrogen within the relative pressure range of 0.4–0.9. This isotherm characteristic was indicative of mesoporous materials possessing narrowly distributed cylindrical mesopores. Specific surface areas, pore volumes, and pore diameters of SBA, CHX@SBA, and CHX@SBA-PDA are shown in Table 1. In comparison to SBA-15, both CHX@SBA and CHX@SBA-PDA exhibited reduced values for all pore parameters. The BET specific surface area of SBA-15 was measured at 489.60 m^2/g, with a BJH estimated pore volume of 1.32 cm^3/g and a pore diameter of 12.05 nm. However, upon loading with CHX, the BET specific surface area decreased to 415.54 m^2/g while the pore diameter reduced to 7.94 nm, indicating successful loading of CHX onto the material. When polydopamine was loaded onto the surface of CHX@SBA, the BET surface area and pore volume were found to be 243.03 m^2/g and 6.39 cm^3/g respectively. In conclusion, polydopamine was successfully coated on CHX@SBA.

3.2 Drug loading and release

Based on the above equation, the drug loading of the nanoparticles was calculated to be 61.5% and the encapsulation rate was 82.74%, which is not much different from the previously reported results (Zhang et al., 2014). The cumulative release rates

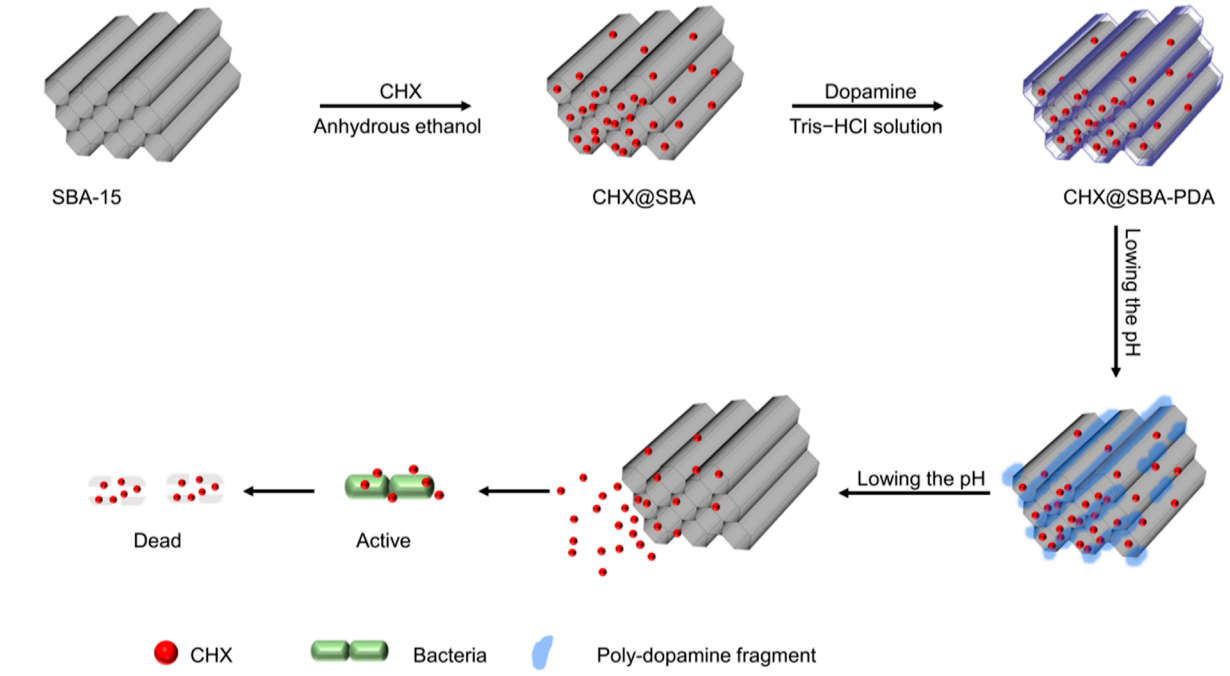

SCHEME 1
Schematic representation of the CHX@SBA-PDA nanoparticles preparation and its antibacterial effect.

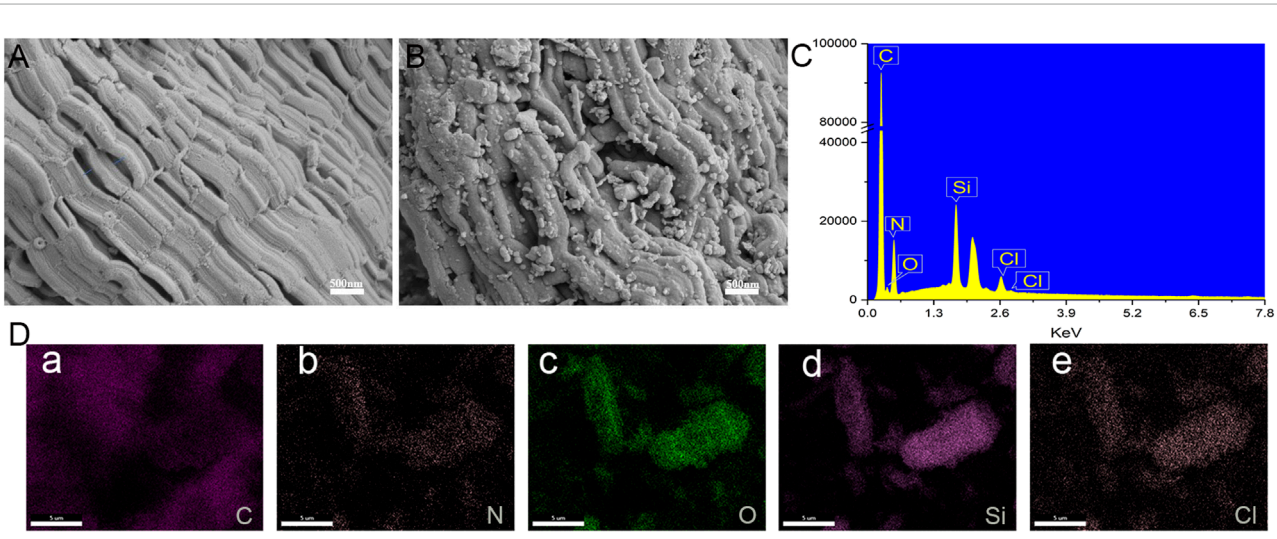

FIGURE 1
SEM characterization of SBA-15 **(A)** and CHX@SBA-PDA **(B)**. Elemental analysis (EDS) of CHX@SBA-PDA **(C)**. Element mapping images of CHX@SBA-PDA **(D)**.

of CHX@SBA and CHX@SBA-PDA are shown in Figure 4. It can be seen that the drug release rate of CHX@SBA-PDA was more pH-dependent compared with that of CHX@SBA. At pH 5.0, the cumulative release rate of CHX@SBA-PDA reached 71.71% within 25 h, which was significantly higher than the 29.22% observed at pH 7.4. Although the release rate of CHX@SBA also exhibited slight pH-dependence, with respective values of 12.97% and 32.38% at pH 7.4 and pH 5.0, which was a small drug release rate with little difference between different pHs. CHX@SBA-PDA exhibited a more significant pH-dependent drug release behavior than CHX@SBA.

3.3 Antibacterial properties

The antibacterial efficacy of modified dentin adhesives is of paramount importance. *Streptococcus mutans*, the primary

TABLE 1 Mesostructural parameters of SBA-15, CHA@SBA, CHX@SBA-PDA.

Samples	Surface area (m^2/g)[a]	Pore volume (cm^3/g)[b]	Pore size (nm)[b]
SBA-15	489.60	1.32	12.05
CHX@SBA	415.54	1.17	7.94
CHX@SBA-PDA	243.03	0.55	6.39

[a]According to BET's algorithm.
[b]According to BJH's algorithm.

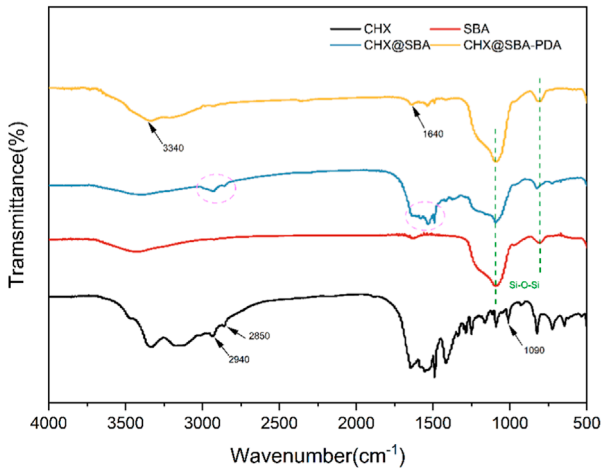

FIGURE 2
FT-IR spectra of CHX, SBA, CHX@SBA, CHX@SBA-PDA.

cariogenic pathogen, was assessed for biofilm formation on the sample surface using antimicrobial assays. The results depicted in Figure 5 illustrate the colony count of *Streptococcus mutans* on modified dentin adhesive plates. Over a period of 24 h and 30 days, an increase in CHX@SBA-PDA content led to a significant reduction in the number of *Streptococcus mutans* ($p < 0.05$). When the CHX@SBA-PDA content reached 2%, an antibacterial rate of 99.81% was achieved within 24 h. Even after 30 days, a remarkable antibacterial rate of 89.84% could still be observed, demonstrating robust and long-lasting antibacterial activity conferred by CHX@SBA-PDA.

The live/dead bacteria kit detects *Streptococcus mutans* adhering to the samples. As shown in Figure 6, there was a significant decrease in the number of viable bacteria on the specimen's surface and a notable increase in dead bacteria as the concentration of CHX@SBA-PDA increased at both 24 h and 30 days time points. When CHX@SBA-PDA reached 1% concentration, virtually no viable bacteria were observed.

Further evaluation of the antibacterial properties of the adhesive revealed that, at the 30 days time point, the unmodified adhesive exhibited dense and uniform colonies. In contrast, the experimental group demonstrated a significant reduction in viable bacteria count, as evidenced by bacterial morphology amplification depicted in Figure 7. The control group displayed a higher number of *Streptococcus mutans* with clear round or oval shapes arranged in double or short chains. However, in the CHX@SBA-PDA group, there was a substantial decrease in live bacteria count along with unclear bacterial morphology characterized by shrinkage, cytoplasmic rupture and leakage of bacterial contents. Moreover, an increase in additive content intensified the disruption of bacterial morphology. These findings further validate the enhanced antibacterial efficacy conferred by modifying the adhesive.

3.4 Shear bonding strength

The adhesive properties of functional adhesives should not be compromised in order to maintain their antibacterial properties. The bond strength of adhesives is a crucial evaluation parameter for resin composites bonded restorations. We employed pH cycling to simulate the model of acid stimulation during normal oral activities. The results of shear strength (MPa) are presented in Table 2. There was no significant difference in shear strength between the control group and artificial saliva at pH 7.4 for 24 h ($p > 0.05$). However, after 30 days of pH cycling, the shear strength decreased by 20.7% and 8.57% for the groups with concentrations of 1 wt% and 2 wt%, respectively. Despite this decrease, their performance remained superior to that of the control group ($p < 0.05$).

The failure mode analysis is presented in Figure 8, revealing that during the two periods of shear strength evaluation, both the hybrid mode and adhesive failure mode were predominant across all groups. The occurrence of mixed failure modes primarily transpires at interfaces where stress distribution is non-uniform. Notably, our findings demonstrate a lack of correlation between bond strength and failure mode, which aligns with our experimental results.

3.5 Cell compatibility

Dental adhesives may exhibit cytotoxicity, which is a crucial consideration for their clinical application. In this study, the cytotoxicity of dental adhesives was assessed by evaluating cell viability and morphology. The CHX@SBA-PDA modified dentin adhesive demonstrated favorable cytocompatibility compared to the control group. As depicted in Figure 9, there was no significant difference in cell viability between each experimental group and the control group after 24 h ($p < 0.05$), indicating that the addition of CHX@SBA-PDA did not enhance adhesive cytotoxicity.

The live and dead cell staining of CHX@SBA-PDA functional adhesive extract cultured for 24 h is shown in Figure 10, which

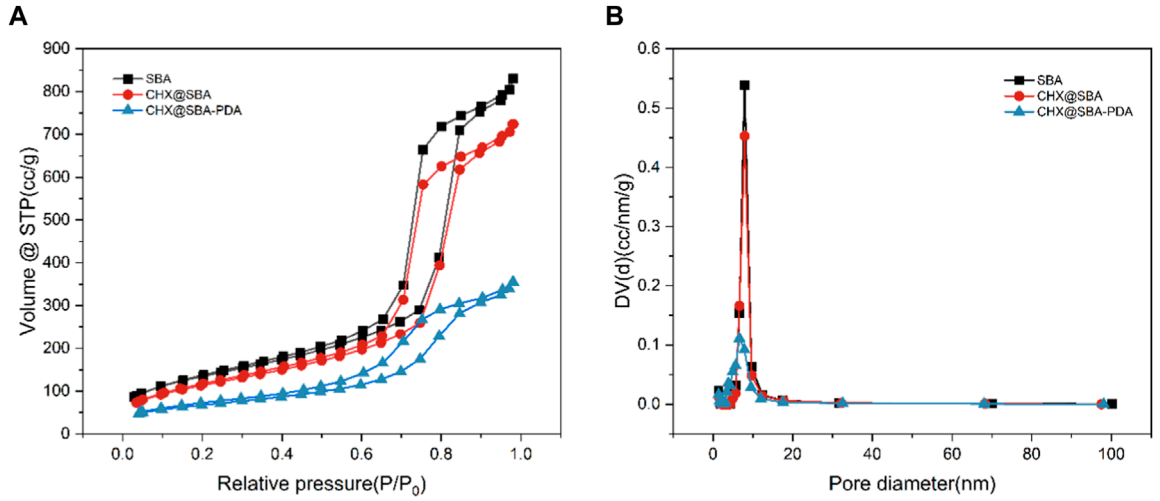

FIGURE 3
(A) Nitrogen adsorption–desorption isotherms of SBA, CHX@SBA, CHX@SBA-PDA. **(B)** Corresponding pore size distribution curves from the Barret–Joyner–Hallender (BJH) adsorption branch.

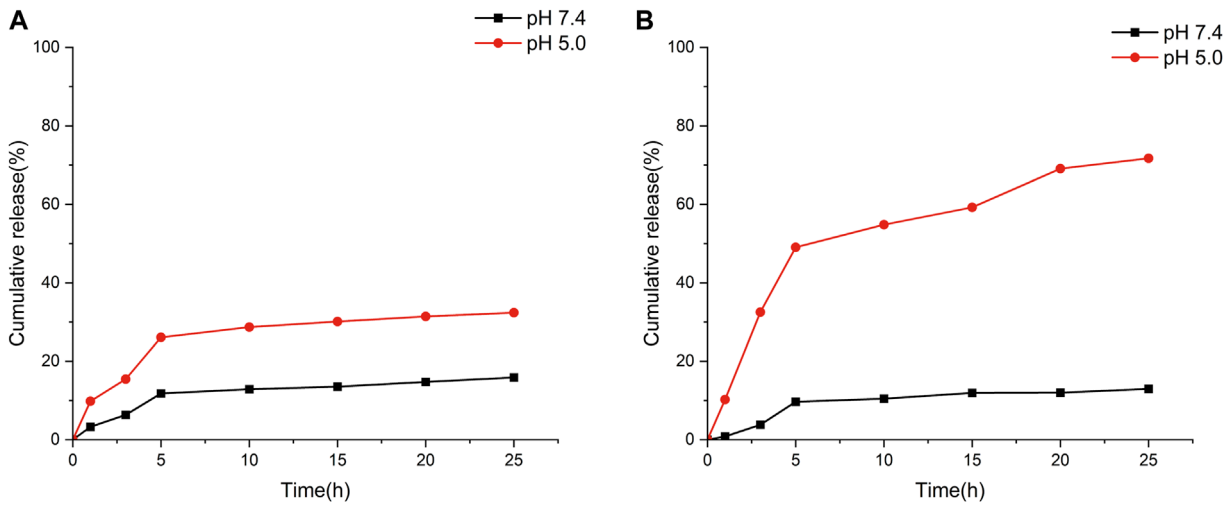

FIGURE 4
In vitro CHX release profiles of CHX@SBA **(A)** and CHX@SBA-PDA nanoparticles at pH 7.4 and 5.0 **(B)**.

TABLE 2 Shear strength (MPa) of functional adhesives after 24 h of artificial saliva storage and 30 days of pH cycling (Mean ± standard deviation).

Groups	24 h in AS (pH 7.4)	30 days in AS (pH7.4/5.0)
0 wt%	20 ± 2Aa	13 ± 2Ab
0.5 wt%	21 ± 3Aa	15 ± 2Bb
1 wt%	21 ± 3Aa	17 ± 2Cb
2 wt%	21 ± 3Aa	20 ± 2Db

Dissimilar uppercase letters (A-D) indicate statistically significant differences in shear strength between groups of adhesives under the same treatment conditions ($p < 0.05$). Dis-similar uppercase letters (a-b) indicates statistically significant differences in shear strength between different treatments for the same group of adhesives ($p < 0.05$).

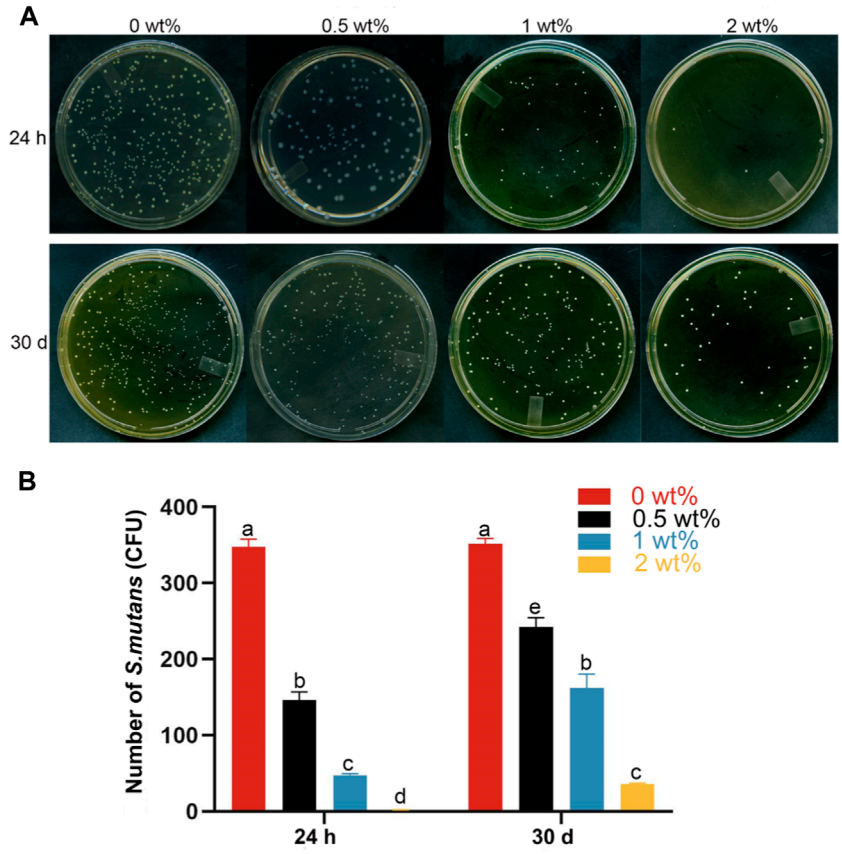

FIGURE 5
Bacterial adhesion plate colony count of the functional adhesive. **(A)** Typical photographs of *Streptococcus mutans* bacterial colonies adhered to dthe surfaces of different functional adhesives. **(B)** Statistical results of *Streptococcus mutans* colony count. Data are shown as mean ± standard deviation (SD). The groups labeled with the same letters have no significant difference ($p > 0.05$).

was consistent with CCK 8 assay. The morphology of HGFs in the experimental group exhibited a favorable fusiform shape, resembling that of the control group, and displayed even distribution. Live/dead staining revealed abundant green-colored live cells and a small number of red-colored dead cells, indicating excellent *in vitro* biocompatibility of CHX@SBA-PDA functional adhesive.

4 Discussion

In this study, CHX@SBA-PDA nanoparticle functional adhesives were developed and their ability to inhibit the growth of *Streptococcus mutans* and prolong the adhesive life of restorations was investigated for the first time. The results demonstrate that CHX@SBA-PDA nanoparticles exhibit pH-controlled smart drug release, excellent biocompatibility and long-term antimicrobial ability, and effectively extend the service life of bonded restorations.

The CHX@SBA-PDA exhibited pH-responsive release properties in contrast to CHX@SBA. This can be mainly attributed to the plydopamine coating, which is primarily assembled through non-covalent bonds. The structure of plydopamine contains a significant number of amino and catechol groups. Under acidic conditions, the amino group becomes protonated, resulting in a positive charge per structural unit of plydopamine. Consequently, electrostatic repulsion occurs leading to dissociation of plydopamine and thus exhibiting high pH sensitivity (Chang et al., 2016; Sapre et al., 2020; Du et al., 2021).

In this study, two types of artificial saliva with different pH levels (7.4 and 5.0) were utilized to simulate the *in vitro* drug release behavior. The selection of these two pH values was based on the fact that pH 7.4 represents the normal physiological conditions of saliva, while pH 5.0 mimics the acidic microenvironment caused by caries bacteria within teeth (Mokeem et al., 2024). These two pH levels simulated both healthy oral conditions and caries-induced oral conditions respectively. At both pH levels, there was no immediate burst release observed for CHX@SBA-PDA nanoparticles due to the presence of plydopamine acting as a gatekeeper on the SBA-15 surface, effectively blocking entry and exit channels for CHX and preventing sudden drug release. Consequently, it can be inferred that CHX@SBA-PDA nanoparticles possess the ability to inhibit premature drug leakage in normal tissues while selectively releasing drugs at targeted sites (van Dijk et al., 2018). The synthesized CHX@SBA-PDA nanoparticles demonstrated potential in inhibiting *Streptococcus*

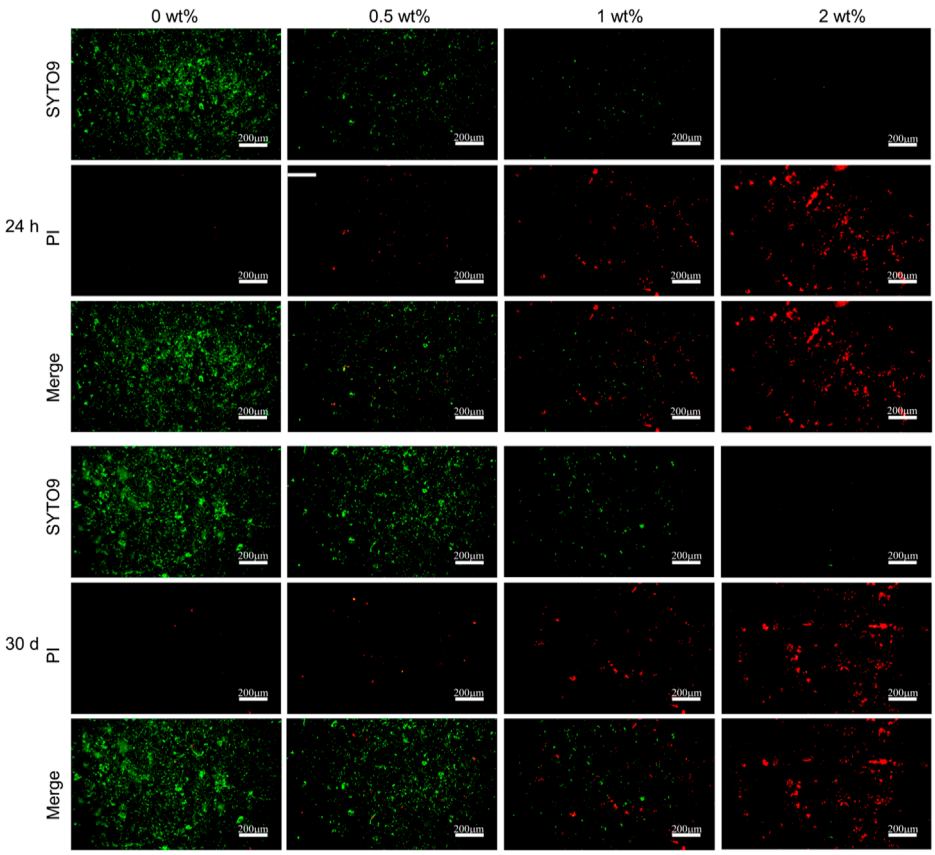

FIGURE 6
Bacterial live/dead fluorescent staining of *Streptococcus mutans* adhered to the adhesive sample (24 h and 30 days).

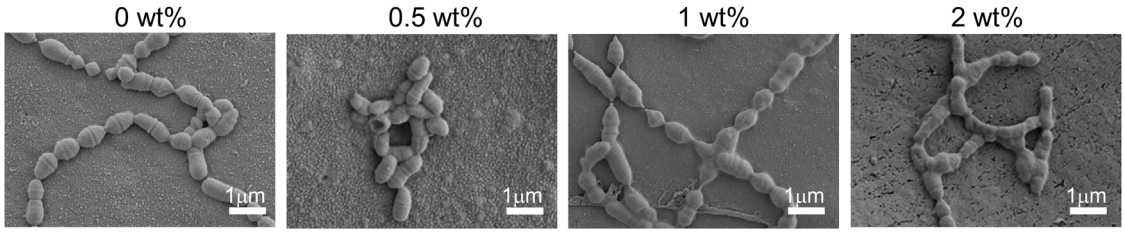

FIGURE 7
Changes in bacterial morphology on the sample surface after 30 days observed by SEM. Bacterial cell membranes in the 0.5 wt% group were significantly constricted. The bacteria in the 1 wt% and 2 wt% groups exhibited cytosolic rupture and leakage of their cytoplasm.

mutans activity, offering promising solutions for addressing resistance-related issues in dental caries treatment (Bai et al., 2019; Kohno et al., 2021).

Streptococcus mutans possesses the ability to produce extracellular polysaccharides from carbohydrates and exhibits acidogenic and acid-resistant properties. As a result, it is regarded as the microbe in dental plaque biofilms that is most cariogenic (Bai et al., 2019). Consequently, *Streptococcus mutans* biological models are extensively utilized in caries research studies. In this experiment, even after 30 days of storage, the addition of 1 wt% and 2 wt% adhesives significantly reduced the activity of *Streptococcus mutans*. This finding is crucial as it indicates the long-lasting antimicrobial effects, which play a vital role in ensuring the sustained clinical success of dental restorative treatments. The long-term antibacterial effect of functional adhesives is attributed to the controlled release of CHX, which destroys the function of the bacterial cell through the coordination of guanidine groups in the bacterial phospholipid cell membrane, thus exerting its bactericidal activity (Muneeswaran et al., 2003). The acidic environment created by bacterial biofilms promotes increased release of CHX from functional adhesives, further enhancing its antibacterial effectivity over time. This pH-sensitive CHX

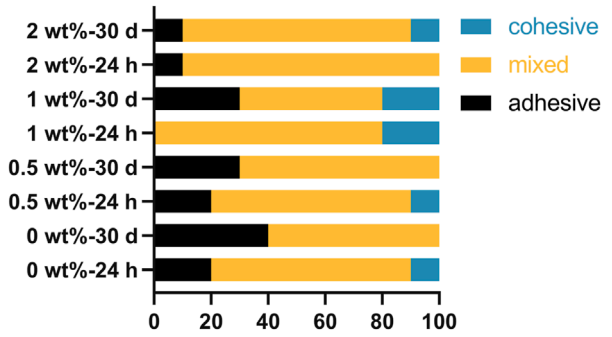

FIGURE 8
Results of fracture pattern analysis of bonded specimens after storage in artificial saliva for 24 h and pH cycling for 30 days.

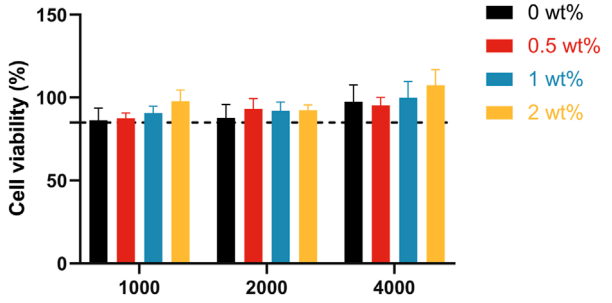

FIGURE 9
The cytotoxicity of the functional adhesive was determined by CCK 8 assay.

release mechanism holds potential implications for combating dentinogenic cariogenic biofilms.

In addition to CHX's antibacterial effectivity through gradual release, plydopamine has been suggested to exhibit contact bactericidal capacity via chelation with ions or proteins as well as electrostatic effects resulting from disruption of bacterial cell membranes (Ma et al., 2023). This dual mechanism may contribute to enhanced antibacterial action when combined with CHX.

The antibacterial properties of functional adhesives should be evaluated for longer time periods (>1 year) to meet clinical needs, as a duration of 30 days is considered short for dental restoration. However, it is important to note the complex role of multi-species oral biofilm in dental caries formation may not be fully replicated only by relying on a single-species *Streptococcus mutans* biofilm model (Sbordone and Bortolaia, 2003; Li et al., 2014). Therefore, further research is required to determine the effects of functional adhesives on multiple cariogenic biofilms.

The antimicrobial properties of functional adhesives should not be compromised at the expense of their adhesive strength, as bond strength is a crucial evaluation parameter for resin composites. The results of this experiment demonstrated no statistically significant difference in the shear strength among the groups at 24 h ($p > 0.05$), which could be attributed to the limited release of CHX in a pH 7.4 environment. Secondary caries does not occur immediately after the placement of restorative materials, necessitating that bonding materials resist acid stimuli encountered in daily oral activities, such as those persisting for a few minutes after each meal or sugar intake. Therefore, an accelerated pH cycling model was employed to simulate the process of the oral cavity being subjected to acid stimulation. Following 30 days of pH cycling, the functional adhesives exhibited higher shear strength compared to the control group ($p < 0.05$), and this enhanced bonding capability was primarily attributed to CHX. Numerous studies have indicated that CHX can enhance dentin bonding *in vitro* by acting as an inhibitor of MMPs, effectively suppressing their activity, reducing collagen fiber degradation, and preserving hybrid layer integrity through competition with MMPs and other metal cations (Lin et al., 2013; Stanislawczuk et al., 2014; Breschi et al., 2020). In an acidic environment at pH 5.0, polydopamine is cleaved resulting in substantial release of CHX, thereby promoting resin-dentin bonding enhancement. Despite significantly improved shear strength after pH cycling with the addition of 2% CHX@SBA-PDA, it remains lower than the bond strength observed at 24 h, further investigation is warranted by increasing nanoparticle dosage.

The evaluation of fracture modes following the shear test revealed that both the hybrid mode and adhesive failure mode were predominant across all groups, with the hybrid failure mode primarily observed at interfaces exhibiting uneven stress distribution (Moule et al., 2007). It has been shown that bond strength is not related to the failure mode (Gurgan et al., 2009; Arslan et al., 2023). This is similar to our experimental results.

The cytotoxicity of dental adhesives is a crucial consideration for their clinical applications. In this study, SBA-15 was utilized as a biocompatible drug carrier, which has demonstrated good compatibility with cells. Additionally, CHX has been proven to be harmless to mammals (Lee et al., 2010) and polydopamine exhibits excellent biocompatibility (Ryu et al., 2018), making it an ideal candidate for biomedical applications. Therefore, the incorporation of CHX@SBA-PDA is speculated not to enhance the adhesive's cytotoxicity. Cell viability and morphology were assessed to evaluate the cytotoxic effects of the adhesives in this study. Both CCK 8 assay and cell live/dead staining revealed high cell viability across all groups, exceeding 85%, surpassing the ISO 10993-5:2009 specified cutoff value of 70%. Furthermore, there were no significant changes observed in terms of cell number or morphology among different adhesive groups, indicating that the addition of CHX@SBA-PDA did not increase adhesive cytotoxicity.

5 Conclusion

In this research, pH-responsive dental adhesive was successfully developed and the experimental results showed that this functional adhesive has long-lasting antimicrobial ability and the addition of nanoparticles does not increase cytotoxicity, which is important for the durability of resin dentin bonding. In conclusion this pH-responsive dental adhesive has potential applications in dental bonding and restoration.

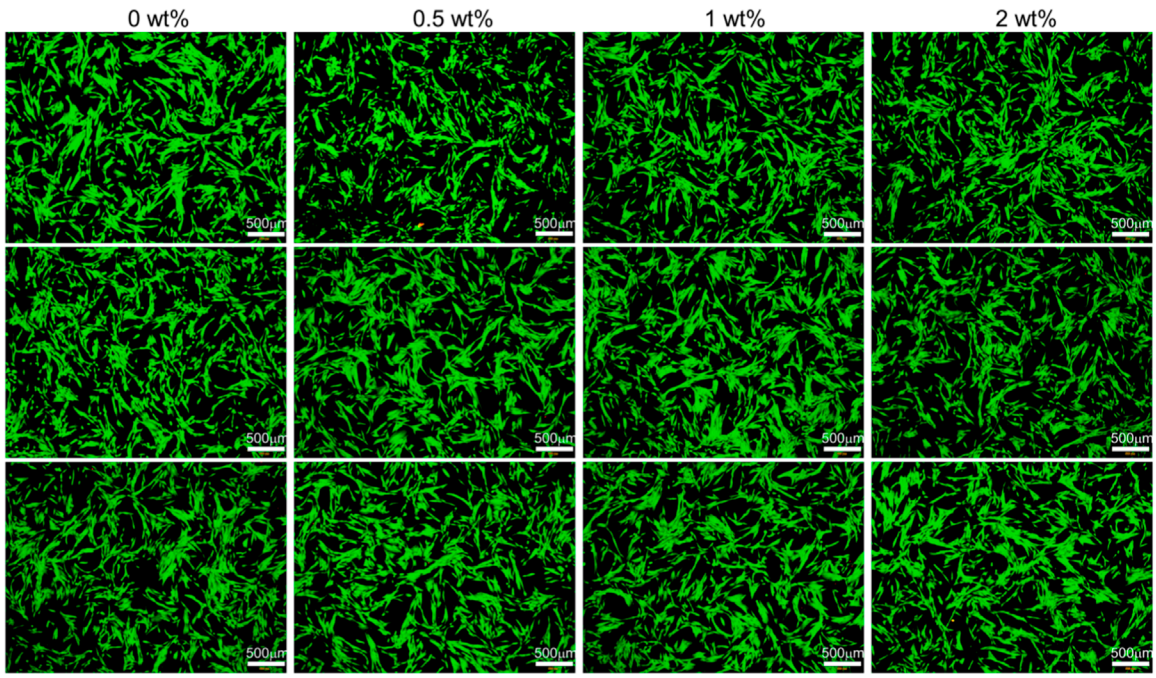

FIGURE 10
Live/dead fluorescent cell staining of human gingival fibroblasts after 24 h of incubation in culture medium (control) and liquid extract of the functional adhesive. Living cells were stained green and dead cells were stained red.

Data availability statement

The original contributions presented in the study are included in the article/supplementary material, further inquiries can be directed to the corresponding author.

Ethics statement

The studies involving humans were approved by the Dental Ethics Committee of Jilin University. The studies were conducted in accordance with the local legislation and institutional requirements. The participants provided their written informed consent to participate in this study.

Author contributions

SL: Writing–original draft, Writing–review and editing. LQ: Formal Analysis, Writing–review and editing. ZL: Funding acquisition, Writing–review and editing.

Funding

The author(s) declare that financial support was received for the research, authorship, and/or publication of this article. This study was funded by Science and Technology Department of Jilin Province (Grant Nos. 20230204076YY, 20220401102YY, and 20210204128YY). This study was funded by National Nature Science Foundation of China (Grant No. 82370934). This study was funded by Changchun Science and Technology Bureau (Grant No. 18YJ010). This study was funded by Project of Rural and Social Development Department of Changchun Science and Technology Bureau (Grant No. 21ZGY01). This study was funded by Major special project of Changchun Science and Technology Bureau (Grant No. 18YJ010). This study was funded by Industrial Technology Research and Development Project of Jilin Provincial Development and Reform Commission (Grant No. 2021C043–2).

Acknowledgments

We would like to express our appreciation to everyone who was involved in the drafting and preparation of the manuscript.

Conflict of interest

The authors declare that the research was conducted in the absence of any commercial or financial relationships that could be construed as a potential conflict of interest.

Publisher's note

References

Abdelmonem, R., Younis, M. K., Hassan, D. H., El-Sayed Ahmed, M. A. E., Hassanein, E., El-Batouty, K., et al. (2019). Formulation and characterization of chlorhexidine HCl nanoemulsion as a promising antibacterial root canal irrigant: *in-vitro* and *ex-vivo* studies. *Int. J. nanomedicine* 14, 4697–4708. doi:10.2147/ijn.s204550

Alansari, N., Abid, M., and Dziedzic, A. (2024). Enhanced antimicrobial efficacy of chlorhexidine-encapsulated halloysite nanotubes incorporated in presurgical orthopedic appliances: an *in vitro*, controlled study. *Clin. oral Investig.* 28 (1), 68. doi:10.1007/s00784-023-05464-7

Anusavice, K. J., Zhang, N. Z., and Shen, C. (2006). Controlled release of chlorhexidine from UDMA-TEGDMA resin. *J. Dent. Res.* 85 (10), 950–954. doi:10.1177/154405910608501016

Arslan, S., Ekrikaya, S., Ildiz, N., Yusufbeyoglu, S., and Ocsoy, İ. (2023). Evaluation of the antibacterial activity of dental adhesive containing biogenic silver nanoparticles decorated nanographene oxide nanocomposites (Ag@nGO NCs) and effect on bond strength to dentine. *Odontology* 112, 341–354. doi:10.1007/s10266-023-00836-7

Bai, Y. M., Mao, J., Li, D. X., Luo, X. J., Chen, J., Tay, F. R., et al. (2019). Bimodal antibacterial system based on quaternary ammonium silane-coupled core-shell hollow mesoporous silica. *Acta biomater.* 85, 229–240. doi:10.1016/j.actbio.2018.12.037

Breschi, L., Maravic, T., Comba, A., Cunha, S. R., Loguercio, A. D., Reis, A., et al. (2020). Chlorhexidine preserves the hybrid layer *in vitro* after 10-years aging. *Dent. Mater. official Publ. Acad. Dent. Mater.* 36 (5), 672–680. doi:10.1016/j.dental.2020.03.009

Budiman, A., Wardhana, Y. W., Ainurofiq, A., Nugraha, Y. P., Qaivani, R., Hakim, S., et al. (2024). Drug-coformer loaded-mesoporous silica nanoparticles: a review of the preparation, characterization, and mechanism of drug release. *Int. J. nanomedicine* 19, 281–305. doi:10.2147/ijn.s449159

Chang, D., Gao, Y., Wang, L., Liu, G., Chen, Y., Wang, T., et al. (2016). Polydopamine-based surface modification of mesoporous silica nanoparticles as pH-sensitive drug delivery vehicles for cancer therapy. *J. colloid interface Sci.* 463, 279–287. doi:10.1016/j.jcis.2015.11.001

Du, J. S., Wang, L. J., Han, X., Dou, J., Jiang, X. F., and Yuan, J. (2021). Polydopamine/keratin complexes as gatekeepers of mesoporous silica nanoparticles for pH and GSH dual responsive drug delivery. *Mater. Lett.*, 293. doi:10.1016/j.matlet.2021.129676

Eltahlah, D., Lynch, C. D., Chadwick, B. L., Blum, I. R., and Wilson, N. H. F. (2018). An update on the reasons for placement and replacement of direct restorations. *J. Dent.* 72, 1–7. doi:10.1016/j.jdent.2018.03.001

Ferracane, J. L. (2017). Models of caries formation around dental composite restorations. *J. Dent. Res.* 96 (4) 364–371. doi:10.1177/0022034516683395

Garcia, I. M., Souza, V. S., Souza, J. D., Visioli, F., Leitune, V. C. B., Scholten, J. D., et al. (2020). Zinc-based particle with ionic liquid as a hybrid filler for dental adhesive resin. *J. Dent.* 102, 103477. doi:10.1016/j.jdent.2020.103477

Geraldeli, S., Maia Carvalho, L. A., de Souza Araújo, I. J., Guarda, M. B., Nascimento, M. M., Bertolo, M. V. L., et al. (2021). Incorporation of arginine to commercial orthodontic light-cured resin cements-physical, adhesive, and antibacterial properties. *Mater. Basel, Switz.* 14 (16), 4391. doi:10.3390/ma14164391

Gurgan, S., Alpaslan, T., Kiremitci, A., Cakir, F. Y., Yazici, E., and Gorucu, J. (2009). Effect of different adhesive systems and laser treatment on the shear bond strength of bleached enamel. *J. Dent.* 37 (7), 527–534. doi:10.1016/j.jdent.2009.03.012

Huang, S., Wu, M., Li, Y., Du, J., Chen, S., Jiang, S., et al. (2022). The dlt operon contributes to the resistance to chlorhexidine in Streptococcus mutans. *Int. J. Antimicrob. agents* 59 (3), 106540. doi:10.1016/j.ijantimicag.2022.106540

Kohno, T., Liu, Y., Tsuboi, R., Kitagawa, H., and Imazato, S. (2021). Evaluation of ion release and the recharge ability of glass-ionomer cement containing BioUnion filler using an *in vitro* saliva-drop setting assembly. *Dent. Mater. official Publ. Acad. Dent. Mater.* 37 (5), 882–893. doi:10.1016/j.dental.2021.02.022

Lee, T. H., Hu, C. C., Lee, S. S., Chou, M. Y., and Chang, Y. C. (2010). Cytotoxicity of chlorhexidine on human osteoblastic cells is related to intracellular glutathione levels. *Int. Endod. J.* 43 (5), 430–435. doi:10.1111/j.1365-2591.2010.01700.x

Li, B., Liao, Y., Su, X., Chen, S., Wang, X., Shen, B., et al. (2023). Powering mesoporous silica nanoparticles into bioactive nanoplatforms for antibacterial therapies: strategies and challenges. *J. nanobiotechnology* 21 (1), 325. doi:10.1186/s12951-023-02093-w

Li, Y., Carrera, C., Chen, R., Li, J., Lenton, P., Rudney, J. D., et al. (2014). Degradation in the dentin-composite interface subjected to multi-species biofilm challenges. *Acta biomater.* 10 (1), 375–383. doi:10.1016/j.actbio.2013.08.034

Lin, J., Kern, M., Ge, J., Zhu, J., Wang, H., Vollrath, O., et al. (2013). Influence of peripheral enamel bonding and chlorhexidine pretreatment on resin bonding to dentin. *J. adhesive Dent.* 15 (4), 351–359. doi:10.3290/j.jad.a29582

Liu, Y., Tjäderhane, L., Breschi, L., Mazzoni, A., Li, N., Mao, J., et al. (2011). Limitations in bonding to dentin and experimental strategies to prevent bond degradation. *J. Dent. Res.* 90 (8), 953–968. doi:10.1177/0022034510391799

Ma, T., Wang, C. X., Ge, X. Y., and Zhang, Y. (2023). Applications of polydopamine in implant surface modification. *Macromol. Biosci.* 23 (10), e2300067. doi:10.1002/mabi.202300067

Mokeem, L. S., Martini Garcia, I., Balhaddad, A. A., Lan, Y., Seifu, D., Weir, M. D., et al. (2024). Multifunctional dental adhesives formulated with silane-coated magnetic Fe(3)O(4)@m-SiO(2) core-shell particles to counteract adhesive interfacial breakdown. *ACS Appl. Mater. interfaces* 16 (2), 2120–2139. doi:10.1021/acsami.3c15157

Moule, C. A., Angelis, F., Kim, G. H., Le, S., Malipatil, S., Foo, M. S., et al. (2007). Resin bonding using an all-etch or self-etch adhesive to enamel after carbamide peroxide and/or CPP-ACP treatment. *Aust. Dent. J.* 52 (2), 133–137. doi:10.1111/j.1834-7819.2007.tb00478.x

Muneeswaran, Z. P., Teoman, B., Wang, Y., Chaudhry, H., Brinzari, T. V., Verma, G., et al. (2003). Novel anionic surfactant-modified chlorhexidine and its potent antimicrobial properties. *Dalton Trans.*, 2024. doi:10.1039/d3dt02559d

Opdam, N. J., Bronkhorst, E. M., Loomans, B. A., and Huysmans, M. C. (2010). 12-year survival of composite vs. amalgam restorations *J. Dent. Res.* 89 (10), 1063–1067. doi:10.1177/0022034510376071

Pitts, N. B., Zero, D. T., Marsh, P. D., Ekstrand, K., Weintraub, J. A., Ramos-Gomez, F., et al. (2017). Dental caries. *Nat. Rev. Dis. Prim.* 3, 17030. doi:10.1038/nrdp.2017.30

Poppolo Deus, F., and Ouanounou, A. (2022). Chlorhexidine in dentistry: pharmacology, uses, and adverse effects. *Int. Dent. J.* 72 (3), 269–277. doi:10.1016/j.identj.2022.01.005

Prado, M. C., Campos, P., Pasetto, S., Marciano, M. A., Sinhoreti, M. A. C., Geraldeli, S., et al. (2023). Development of nanobiosilicate, tricalcium phosphate and chlorhexidine materials for biomineralization with crystallographic similarity to hydroxyapatite and biomodified collagen. *Dent. Mater. official Publ. Acad. Dent. Mater.* 40, 267–275. doi:10.1016/j.dental.2023.11.015

Ryu, J. H., Messersmith, P. B., and Lee, H. (2018). Polydopamine surface chemistry: a decade of discovery. *ACS Appl. Mater. interfaces* 10 (9), 7523–7540. doi:10.1021/acsami.7b19865

Sapre, N., Chakraborty, R., Purohit, P., Bhat, S., Das, G., and Bajpe, S. R. (2020). Enteric pH responsive cargo release from PDA and PEG coated mesoporous silica nanoparticles: a comparative study in *Drosophila melanogaster*. *RSC Adv.* 10 (20), 11716–11726. doi:10.1039/c9ra11019d

Sbordone, L., and Bortolaia, C. (2003). Oral microbial biofilms and plaque-related diseases: microbial communities and their role in the shift from oral health to disease. *Clin. oral Investig.* 7 (4), 181–188. doi:10.1007/s00784-003-0236-1

Simecek, J. W., Diefenderfer, K. E., and Cohen, M. E. (2009). An evaluation of replacement rates for posterior resin-based composite and amalgam restorations in U.S. Navy and marine corps recruits. *J. Am. Dent. Assoc. (1939)* 140 (2), 200–209. quiz 49. doi:10.14219/jada.archive.2009.0134

Solderer, A., Kaufmann, M., Hofer, D., Wiedemeier, D., Attin, T., and Schmidlin, P. R. (2019). Efficacy of chlorhexidine rinses after periodontal or implant surgery: a systematic review. *Clin. oral Investig.* 23 (1), 21–32. doi:10.1007/s00784-018-2761-y

Spencer, P., Ye, Q., Park, J., Topp, E. M., Misra, A., Marangos, O., et al. (2010). Adhesive/Dentin interface: the weak link in the composite restoration. *Ann. Biomed. Eng.* 38 (6), 1989–2003. doi:10.1007/s10439-010-9969-6

Stanislawczuk, R., Pereira, F., Muñoz, M. A., Luque, I., Farago, P. V., Reis, A., et al. (2014). Effects of chlorhexidine-containing adhesives on the durability of resin-dentine interfaces. *J. Dent.* 42 (1), 39–47. doi:10.1016/j.jdent.2013.11.002

Stewart, C. A., Hong, J. H., Hatton, B. D., and Finer, Y. (2018). Responsive antimicrobial dental adhesive based on drug-silica co-assembled particles. *Acta biomater.* 76, 283–294. doi:10.1016/j.actbio.2018.06.032

Takahashi, N., and Nyvad, B. (2011). The role of bacteria in the caries process: ecological perspectives. *J. Dent. Res.* 90 (3), 294–303. doi:10.1177/0022034510379602

Takamori, D. Y., Bizeto, M. A., de Abreu Fantini, M. C., Lacerda Rubinger, C. P., Faez, R., and Martins, T. S. (2019). Polyaniline inclusion into ordered mesoporous silica

matrices: synthesis, characterization and electrical transport mechanism. *Microporous Mesoporous Mater.* 274, 212–219. doi:10.1016/j.micromeso.2018.07.045

van Dijk, F., Teekamp, N., Beljaars, L., Post, E., Zuidema, J., Steendam, R., et al. (2018). Pharmacokinetics of a sustained release formulation of PDGFβ-receptor directed carrier proteins to target the fibrotic liver. *J. Control. release official J. Control. Release Soc.* 269, 258–265. doi:10.1016/j.jconrel.2017.11.029

Williams, D. M. (2014). The research agenda on oral health inequalities: the IADR-GOHIRA initiative. *Med. Princ. Pract. Int. J. Kuwait Univ. Health Sci. Centre* 23, 52–59. doi:10.1159/000356934

Wu, M., Wang, Q., Peng, Y., Liang, X., Lv, X., Wang, S., et al. (2023). Enhancing targeted therapy in hepatocellular carcinoma through a pH-responsive delivery system: folic acid-modified polydopamine-paclitaxel-loaded poly(3-hydroxybutyrate-co-3-hydroxyvalerate) nanoparticles. *Mol. Pharm.* 21, 581–595. doi:10.1021/acs.molpharmaceut.3c00710

Wu, M., Zhong, C., Zhang, Q., Wang, L., Wang, L., Liu, Y., et al. (2021). pH-responsive delivery vehicle based on RGD-modified polydopamine-paclitaxel-loaded poly (3-hydroxybutyrate-co-3-hydroxyvalerate) nanoparticles for targeted therapy in hepatocellular carcinoma. *J. nanobiotechnology* 19 (1), 39. doi:10.1186/s12951-021-00783-x

Xu, B., Li, S., Shi, R., and Liu, H. (2023). Multifunctional mesoporous silica nanoparticles for biomedical applications. *Signal Transduct. Target. Ther.* 8 (1), 435. doi:10.1038/s41392-023-01654-7

Yan, H., Yang, H., Li, K., Yu, J., and Huang, C. (2017). Effects of chlorhexidine-encapsulated mesoporous silica nanoparticles on the anti-biofilm and mechanical properties of glass ionomer cement. *Mol. Basel, Switz.* 22 (7), 1225. doi:10.3390/molecules22071225

Zhang, J. F., Wu, R., Fan, Y., Liao, S., Wang, Y., Wen, Z. T., et al. (2014). Antibacterial dental composites with chlorhexidine and mesoporous silica. *J. Dent. Res.* 93 (12), 1283–1289. doi:10.1177/0022034514555143